Journal of Marine Science and Technology

Volume 22 | Issue 2 Article 7

THE NUMERICAL STUDY OF THE DYNAMIC BEHAVIOR OF AN UNDERWATER VEHICLE

Tsung-Lung Liu
Department of Power Vehicle and Systems Engineering, CCIT, National Defense University, Taoyuan, Taiwan, R.O.C, tlliu@ndu.edu.tw

Kuan-Cheng Pan
School of Defense Science, CCIT, National Defense University, Taoyuan, Taiwan, R.O.C

Recommended Citation

Liu, Tsung-Lung and Pan, Kuan-Cheng (2014) "THE NUMERICAL STUDY OF THE DYNAMIC BEHAVIOR OF AN UNDERWATER VEHICLE," *Journal of Marine Science and Technology*: Vol. 22: Iss. 2, Article 7.
DOI: 10.6119/JMST-013-0207-5
Available at: https://jmstt.ntou.edu.tw/journal/vol22/iss2/7

Journal of Marine Science and Technology, Vol. 22, No. 2, pp. 163-172 (2014)
DOI: 10.6119/JMST-013-0207-5

THE NUMERICAL STUDY OF THE DYNAMIC BEHAVIOR OF AN UNDERWATER VEHICLE

Tsung-Lung Liu[1] and Kuan-Cheng Pan[2]

Key words: underwater vehicle, computational fluid dynamics (CFD), dynamic mesh technique, unsteady flow.

ABSTRACT

How to employ numerical methods to predict the dynamic behavior of underwater vehicles will become important in the near future. Over the past decade, the results obtained from the Computational Fluid Dynamics (CFD) methods had been proven similar to that of experimental approach with the same test conditions. In order to reduce the computational time of such flow simulation, the concept of relative motion with body-fixed and fluid-moving scheme is usually employed as a conventional procedure to figure out the flow physics around moving bodies. However, the dynamic influence of fluid on a moving vehicle is self-evident and the relative motion mode of CFD can not fully capture the flow physics around the vehicle. To reveal the dynamic behavior of underwater vehicles, the dynamic mesh technique was applied in the present research for capturing the interaction between the moving body and fluid. Based on the mesh regeneration and interpolation techniques, the present numerical method which is very practical for the unsteady flow computation could be used to predict the trajectory of a moving body. Furthermore, it also could benefit ocean engineers to predict the maneuvering capability of a modern underwater vehicle.

I. INTRODUCTION

Even now, most of the oceans still remain as mysterious place humans are drawn to explore. Today, with the gradual depletion of the globe's finite land resources and the corresponding demand to develop new potential resources, humans have been forced to explore and exploit the oceans. For multiple reasons, including to retain their leadership in the coming global competition for marine resources, industrialized nations have heavily invested in the development of marine technology. Compared with conducting large construction or surface drilling projects on land, which can be often supervised and operated well at all times, performing underwater engineering is rife with uncertainty and danger, especially using manned vehicles for deep sea projects. In addition to the load and space considerations for crew, the life support and power systems required for the operation of manned underwater vehicles cannot be overlooked. Thus, these limitations should substantially increase the difficulty of research and development of small manned underwater vehicles and provide a broad development space for unmanned underwater vehicles.

Unmanned underwater vehicles (UUVs) refer to all underwater vehicles or operational units that operate without carrying any person. The main feature of UUVs is that pilots are no longer required. This feature makes it suitable for fulfilling extremely dangerous underwater tasks at water depths unreachable by humans. Generally, UUVs can be divided into two categories according to their operational model: cabled remotely operated vehicles (ROVs) and un-cabled autonomous underwater vehicles (AUVs). The primary difference between them is that during operation, ROVs must maintain a connection to its mother ship with a cable for command transmission and control purposes; thus, ROVs are relatively slow with poor mobility and a limited range of operations. AUVs, however, do not depend on a cable for control; the complete system can be preset prior to operation. AUVs execute the specific job according to the preset route and automatically return to the preset location to rejoin the mother ship after assigned missions are completed. ROVs and AUVs have innate differences. Although both of them are employed to explore the underwater environment, each has its own specialty and area of application which can be depicted with Fig. 1.

Because AUVs can detect and act autonomously without human intervention during operations, they can be used to do many scientific researches such as marine environmental surveys, hydrological data collection, and underwater environmental monitoring etc. In addition to scientific tasks, they can also be employed for construction projects such as setting seafloor power cables and pipes and the construction and maintenance of underwater structures. Moreover, AUV technology has been rapidly developed for military purposes.

Paper submitted 03/13/12; revised 01/10/13; accepted 02/07/13. Author for correspondence: Tsung-Lung Liu (e-mail: tlliu@ndu.edu.tw).
[1] Department of Power Vehicle and Systems Engineering, CCIT, National Defense University, Taoyuan, Taiwan, R.O.C.
[2] School of Defense Science, CCIT, National Defense University, Taoyuan, Taiwan, R.O.C.

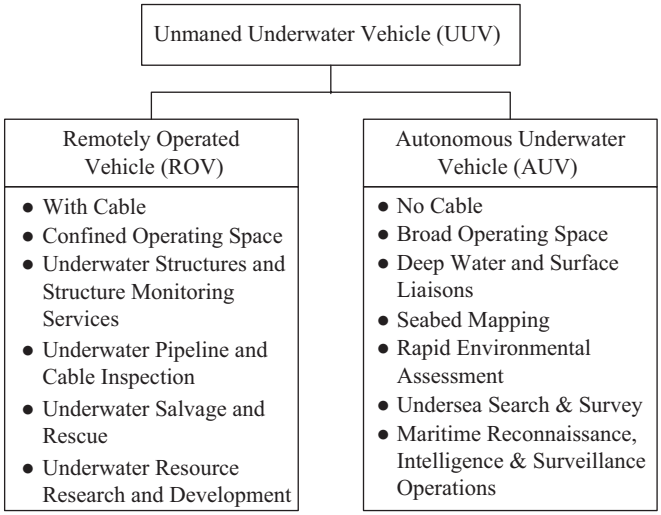

Fig. 1. Classification and characteristic of UUVs.

They could be applied to perform mine-disarmament, special force support, anti-submarine warfare, and underwater reconnaissance and surveillance. All the world's advanced nations have noticed the potential of their military application and heavily financially invested in the research and development of these new weapons, which could likely dominate the future underwater warfare [2, 8].

There is no doubt that the mobility and guidance control related to the maneuvering performance are important for AUV design. To predict the sailing trace of an AUV, the Computational Fluid Dynamics (CFD) technique could be employed to compute the vehicle's moving resistance and examine the dynamic influence of its control fin on the vehicle. After decades of development, the CFD techniques have been regarded as useful tools to provide simulation results similar to those obtained from experimental methods. Regarding the application of CFD mentioned previously, two computational options, namely, absolute and relative motion modes are often adopted to explore the flow physics around the moving vehicles. Compared with the relative one, the use of absolute mode could provide more realistic analysis for the numerical flow simulation. There are some interesting facts that can be revealed by means of absolute mode computation. However, it takes more simulation time for the absolute mode computation than the relative one. So far the majority of researches on the flow fields around vehicles still employ the relative mode of CFD simulation which was completed with specific flow speed fluid flowing around a stationary research object. Therefore, before focusing on a closer discussion about the use of absolute mode, a few papers should be referred concerning the relative mode. Chen *et al*. [5] used CFD technology to simulate the motion properties of a micro-underwater vehicle and, after verifying the results using empirical data, identified the relationship between vehicle's hydrodynamic properties such as resistance etc. and its moving speed. Pan and Huang [12] used Fluent software to analyze and compare cylindrical and semi-cylindrical underwater vehicles. They discovered that cylindrical vehicles were better to resist pressure and that an attack angle less than -5° would increase a vehicle's dive efficiency. Furthermore, both simulated and empirical data for different speeds showed that lift is approximately 0 as the attack angle is between -2° and -2.5°, where the vehicle can retain a stable forward motion. However, these concepts are not suitable for predicting the effect of the control fin motion on the vehicle's moving trace. To increase the accuracy of the simulated object motion scenarios, researchers observed and explored the physical phenomena during the actual motion of an object in an unstable flow and then developed the dynamic mesh technique. Regarding dynamic mesh techniques in the research and application of submerged underwater bodies, Liu *et al*. [11] have implemented these techniques to investigate the motion behavior of torpedoes and submarines in water. After analyzing the resistance of submerged moving objects, comparison and verification with the experimental values were conducted. The results show that dynamic mesh techniques could become effective methods for examining the motion behavior of submerged underwater bodies.

Generally, the dynamic analysis of the moving underwater vehicle must conform to the researcher's simulation concept. Additionally, the solution solved by the combined fluid governing and body motion equation within the executed computations must answer the moving position of the object during the simulation. Actually, it is not difficult to determine the displacement position of the simulated object once the total external force on the object is calculated. However, because of the essence of the numerical method, the moving bodies are often enclosed by a large quantity of flow meshes for their dynamic flow simulation. Therefore, in addition to calculating the displacement of the body, how to regenerate the flow meshes enclosing the moving object is always a challenging issue. As discussed previously, calculation accuracy is closely related to the quality of the flow meshes in the computational domain. Thus, manipulating the mesh regeneration problem appropriately could be the most crucial component that affects the accuracy and efficiency of the simulation. Currently, numerical methods considering the effect of viscosity can be combined with mesh-regeneration or dynamic mesh technique for the dynamic simulation of moving bodies [3, 7]. The major breakthrough of this technology is that it enables even more useful applications of numerical simulation methods for engineering design. To improve the design capabilities of underwater vehicles, this study would apply the dynamic mesh technique to evaluate the maneuvering capability of the AUV. Moreover, the simulations conducted by the present research would investigate all possible dynamic motion behavior affected by the control fin surface. Compared to the relative mode that usually has been chosen previously, the dynamic mesh technique could be applied nowadays to reveal more subtle physical phenomenon related to vehicle motion and further improve the underwater vehicle design capabilities for ocean engineers.

Fig. 2. Photo of SeaOtter Mk I [1].

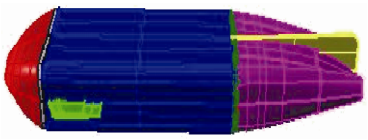

Fig. 3. CAD graph of SeaOtter Mk I.

II. AUV CONFIGURATION DESIGN

For the configuration design of the simulated vehicle, SeaOtter MK I (Fig. 2) manufactured by Atlas Maridan Inc. [1] has been referred in the present study. The geometry design with reasonable simplification of SeaOtter MK I was done by the use of CAD software Rhino and its modified configuration can be seen in Fig. 3. The geometry simplification will facilitate the simulation of AUV flow computation.

III. THE NUMERICAL METHODS FOR FLOW FIELD SIMULATION

1. Governing Equations and Numerical Methods

To simulate the complex flow field of AUV, based on related literature, this study used the Reynolds Averaged Navier-Stokes (RANS) equations as the governing equations to solve the viscous flow around the vehicle. In the present research, FLUENT CFD code which employs the finite volume method (FVM), standard k-ε, and dynamic mesh technique to solve RANS equations has been employed for the dynamic behavior simulation of AUV. The RANS equations in the tensor form of the orthogonal curvilinear coordinate system can be written as follows [4]:

$$\sum_{i=1}^{3} \frac{\partial U_i}{\partial x^i} = 0 \tag{1}$$

$$\frac{\partial U_i}{\partial t} + \sum_{j=1}^{3} \left(U_j \frac{\partial U_i}{\partial x^j} + \frac{\partial \overline{u_i u_j}}{\partial x^j} \right) + \frac{\partial p}{\partial x^i} - \frac{1}{\mathrm{Re}} \nabla^2 U_i = 0 \tag{2}$$

where U_i represents the average velocity, p is pressure, Re = U_0/v represents the Reynolds number, and $\overline{u_i u_j}$ represents the Reynolds stress. The presence of Reynolds stress prevents the equation from closing. Therefore, this study substituted the Reynolds stress in Eq. (2) with the k-ε turbulence model, where the number of unknown values in the equation was identical to the number of equations. Then, the FVM discrete flow field governing equations can be applied. For the physical calculations of flow field related to an object's motion in fluid, this study applied the Fluent 6.3 flow computation commercial software platform with dynamic mesh treatment technology and the object's six-degrees-of-freedom motion equation to calculate the underwater vehicle's dynamic motion flow field.

Flow field dynamic mesh treatment technology has matured and been verified by previous studies as an effective method for calculating an object's dynamic motion in fluid. Because dynamic mesh can effectively manage mesh-regeneration problems that arise following body motion, the surrounding mesh connected to the body surface can be used to adjust the distance of the mesh from the boundary mesh point according to the amount of body motion. After new coordinates are allocated to the surrounding mesh points near the body surface, the surrounding mesh points connected to the body surface readjust their positions accordingly, thereby preventing mesh overlaps. The general principles of this technology assume that the sides of each mesh within the computational domain can be considered a spring with some ability to stretch and contract. Changes in the distance between mesh points can be regarded as the space created by the extension of a spring between mesh points. Therefore, after defining the elasticity coefficient, the amount of adjustment required for mesh point movement can be determined using the concepts of Hook's Law. After determining new coordinates of each mesh point in the calculation area, the physical quantities in the flow field obtained previously can be interpolated into the calculation area composed of new mesh points. Consequently, after satisfying the boundary conditions of each physical quantity in the flow field at the boundary of the moving body, each physical quantity in the flow field at the present time can be iteratively calculated using the resulting interpolated value as the initial condition for the next time step computation. Actually, the change in displaced space by the moving object in the flow field often distorts the flow field meshes around the object. To maintain the mesh quality in the computational domain, the size of the distortion must be adjusted according to the distance of the object's motion or the size of their rotational angle. When the mesh side distortion skews excessively, and if the simulation accuracy cannot be improved by just readjusting the length of the mesh sides, the sides must be cut to regenerate the new meshes to meet the requirement for flow computation. Once the mesh is regenerated, the mesh size should be standardized to avoid the waste of computational time to grow useless meshes. The readers are referred to good tutorial in Fluent 6.3 user manual [6] for an introduction to the above approach and its application.

2. Verification of Numerical Results

This study combined a flow solver, dynamic mesh, and six-degrees-of-freedom motion solver to predict the dynamic motion behavior of AUVs. Due to lack of experimental data

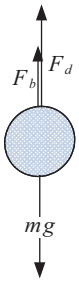

Fig. 4. Schematic diagram of the forces acting on a moving sphere.

for the verification of AUV flow simulation, the test cases of a spherical dropping down in various liquid have been studied. The velocity, acceleration, and displacement of the moving object obtained from the case studies were compared with the results from empirical formulae to verify the accuracy of the research methods.

When simulating the free falling motion of a spherical object, we assumed that a spherical object with mass m would drop down freely from rest in liquid with a density of ρ, (Fig. 4). Then, gravity force mg in the same direction as the object's motion and resistance F_d and buoyant force F_b in the opposite direction of the object's motion are exerted on the object. The motion equation of the spherical object can be expressed as follows:

$$\sum F = mg - F_d - F_b = ma \tag{3}$$

where a denotes acceleration and ΣF is resultant of forces. Meanwhile, in Eq. (3), resistance F_d and buoyancy F_b can be expressed as $F_d = 0.5\rho v^2 C_d A$ and $F_b = \forall \rho g$ respectively, where ρ is fluid density, v is the object's velocity of descent, C_d is the resistance coefficient, A is the object's surface area, and $\forall$ is the object's volume. Because the object's initial velocity is zero, Eq. (3) can be rewritten as follows:

$$\begin{cases} v = at \\ mg - \dfrac{1}{2}\rho v^2 C_d A - \forall \rho g = ma \end{cases} \tag{4}$$

Thus, by including the relevant coefficient values from each empirical formula, the simultaneous equations in Eq. (4) can be solved to obtain each relevant kinetic quantity of a free falling object.

Figs. 5 and 6 show the simulation results of a sphere dropping down in air and water respectively for 1.8 sec. In the present simulation the dynamic mesh technique was employed to calculate the sphere dynamic motion and regenerate the mesh surrounding the sphere shown as Figs. 5(a) and 6(a). The simulation results for the pressure field distribution around the spheres are presented in Figs. 5(b) and 6(b). As for the setting of the boundary conditions (BCs) in these test examples, detailed information is described as follows: (1)

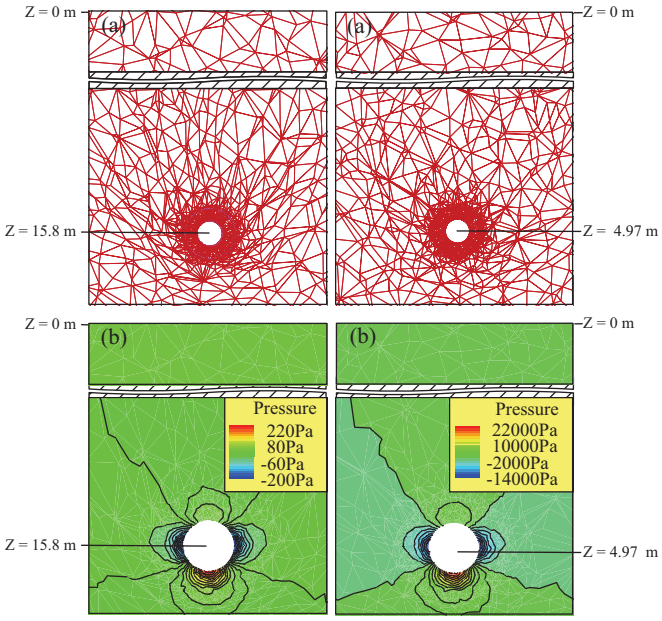

Fig. 5. Simulation for sphere motion in air (a) mesh regeneration (b) pressure field around a sphere.

Fig. 6. Simulation for sphere motion in water (a) mesh regeneration (b) pressure field around a sphere.

symmetry BC for the upper and side boundaries of the computational domain; and (2) wall BC for the lower boundary and sphere surface. Regarding the geometric and material natures of the test object, the free-falling body within the computational domain was set as an iron sphere with a radius of 0.1 m, a mass of 32.966 kg, and moment of inertias Ixx = Iyy = Izz equaling to 0.132 kg · m^2. Meanwhile, in this calculation, the geometric configuration of the computational domain surrounding the sphere is cylindrical, and the usage of mesh numbers contained in computational domain is 519,795.

As also shown in Figs. 5 and 6, the distance covered by the sphere falling for 1.8 sec of simulated time was significantly greater in air than that in water. This difference is caused by the significantly greater viscous forces exerted on the sphere in water. Furthermore, to improve the simulation accuracy for the computation of flow field around the sphere, fine meshes were constructed around the sphere to facilitate mesh regeneration when the sphere was in motion. The pressure contours around the moving sphere showed in Figs. 5(b) and 6(b) also indicate that the greatest pressure is distributed on the front portion of the sphere during the drop, and the pressure gradually decreases toward the back of the sphere before increasing again. Obviously, the numerical result matches the flight phenomenon of an aerial vehicle, where the lead edge of the control fin bears the greatest pressure. In summary, the simulation results obtained from the test cases mentioned above not only conforms to the kinetic physics of a free falling object but can also demonstrate the availability of dynamic mesh technique. Therefore, using

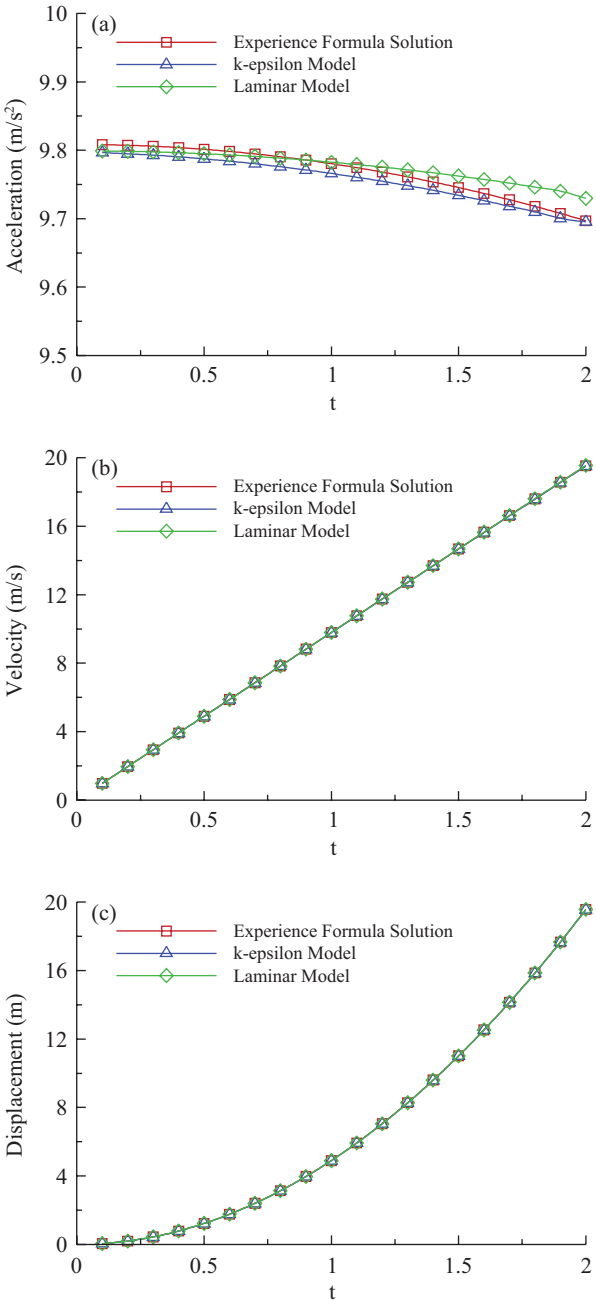

Fig. 7. Comparisons of acceleration, velocity and displacement of a sphere dropping downward in air.

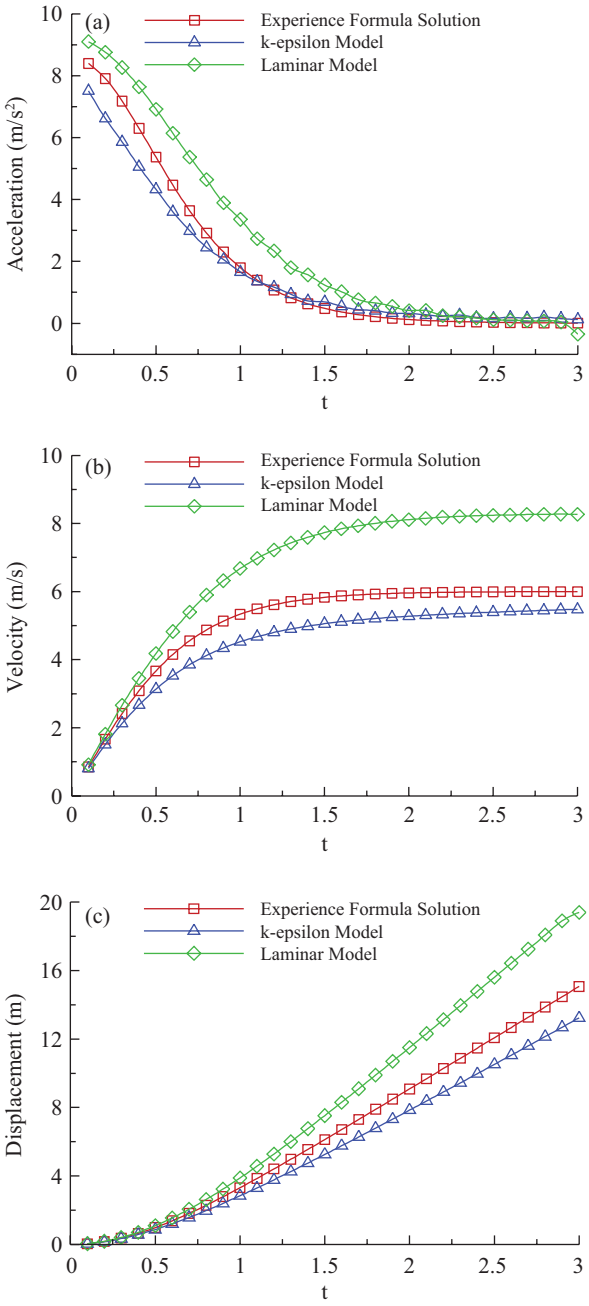

Fig. 8. Comparisons of acceleration, velocity and displacement of a sphere dropping downward in water.

mesh regeneration technique to analyze the motion behavior of underwater vehicles could be likely to produce meaningful results for their design.

Figs. 7 and 8 illustrate the corresponding relationship between the physical motion and time measurements of a sphere free falling in air and water. Additionally, Figs. 7 and 8 compare the results obtained from empirical formula and different numerical methods including laminar and turbulence computations. Fig. 7 clearly shows that minimal differences exist between the numerically-calculated and empirical formula results of a sphere moving in air, verifying that numerical method could provide good results. Fig. 8 shows that the simulated results obtained from the k-ε turbulence model are relatively closer to the empirical formula than those obtained from the laminar model. The reason for this is that the Reynolds number is larger for a sphere moving through water than through air. Therefore, the usage of k-ε turbulence model could provide better results. Overall, although the numerical results differed significantly from those of the empirical formula, their curves' tendencies shown in

Table 1. Dimensions and physical quantities of AUV.

Dimensions			
Length (m)	Width (m)	Height (m)	
4.50	1.18	0.59	
Physical Quantities			
Mass (kg)	I*xx* (kg · m^2)	I*yy* (kg · m^2)	Izz (kg · m^2)
1500.00	201.38	1865.45	1987.95

Figs. 8(a)-8(c) are extremely similar. In addition, It should be noted that because the sphere's dropping speed and displacement in air are greater than that in water, the maximum value on the vertical and horizontal axes shown in Figs. 7(b)-7(c) is the largest and the smallest respectively as compared with those in Figs. 8(b)-8(c). Therefore, to ensure size uniformity between Figs. 7 and 8, the scale ratios of vertical axis to horizontal axis used in Figs. 7(b)-7(c) are larger than those used in Figs. 8(b)-8(c), therefor making the numerical and empirical formula curves in Figs. 7(b) and 7(c) to overlap more or less.

In summary, the results of the mesh regeneration technique for a free falling object in air and water were generally consistent with that of the empirical formula. This consistency confirms that the analysis method can effectively analyze the motion characteristics of a vehicle in water and better predict its motion behavior.

3. Computational Domain Dimensions and Specification of BCs for AUV Flow Simulation

The principal dimensions and dynamic quantities of the underwater vehicle studied in the present research are shown in Table 1. Meanwhile, the dimensions of the computational domain are 90 m length × 30 m width × 40 m height. Regarding the effect of domain size on the submerged-body flow, Lin [9] has employed the present numerical method to investigate the influence of wall effect on the torpedo flow. The results reported by Lin [9] suggest that when the width of the flow field calculation area is 25 times the diameter of a submerged underwater body, the flow field around the submerged object is, obviously, not influenced by the tank wall effect. Lin's study could serve as the basis for determining the dimensions of the computational domain. Thus, following up the implications concluded by Lin [9] the choice of the computational domain in the present study can mitigate the influence of the tank wall effect, thereby providing a simulation result that is closer to reality. Furthermore, with regard to the construction of the computational domain for the present study, the mesh generation software Gridgen has been used to generate the flow field meshes that encompass a moving AUV. To deal with the mesh regeneration problems focused on the region nearby the moving body, the computational domain was divided into two sections: (1) the moving block enveloping the body without relative motion between meshes and the body, and (2) computational block excluding

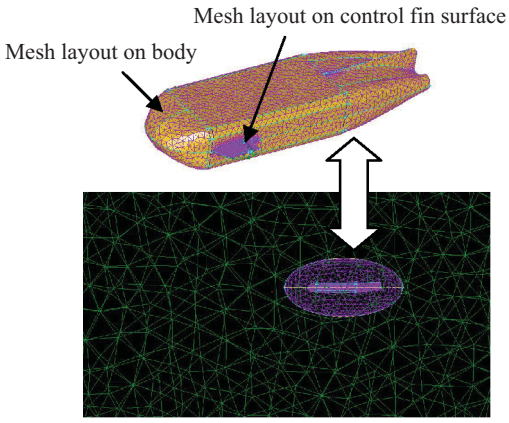

Fig. 9. Schematic diagram for mesh layout on AUV and computational domain.

the block surrounding AUV so as the dynamic mesh technique can be applied to do the dynamic motion simulation of the AUV. This computational domain mesh division is shown in Fig. 9.

When constructing meshes for flow simulation, the mesh quality and mesh amount are the two primary factors that directly affect the numerical calculation result. Mesh with low skewness and high quality can provide more precise numerical calculation results. However, the consequent could significantly increase in mesh amount and double the calculation time. Thus, a trade-off between the mesh amount and mesh quality must be made based on the computational capacity of existing computer equipment and the purpose of numerical calculations. This enables the research objective to be achieved in the shortest amount of time using limited resources.

To maintain the quality of the meshes surrounding the AUV, fine meshes are used and do not regenerate in the moving block that envelops the AUV. The moving block would move with the same velocity as the AUV. Conversely, for the purpose of reducing the simulation time, coarse meshes are employed in the region excluding the moving block. In this region, mesh regeneration would take place as long as the AUV moves to compress or stretch the meshes nearby the moving block. For the moving block encompassing the AUV, the usage of mesh numbers are 127,250. As for the computational domain excluding the AUV block, 196,071 meshes are used for a total number of 323,321 meshes in this study. Meanwhile, the smallest mesh volume is 2.860151×10^{-8} m^3 and the largest is 2.955527 m^3 which can be found in the in the computational domain.

This study employed the dynamic mesh technique to simulate the six-degree motion of AUV. As for setting of boundary conditions (BC) of a moving AUV within the computational domain, the no-slip BC was set on the surface of the marine vehicle. Also, the sea bottom boundary was a solid boundary and was set as a non-slip boundary condition. To shorten the computing time required to perform the numerical

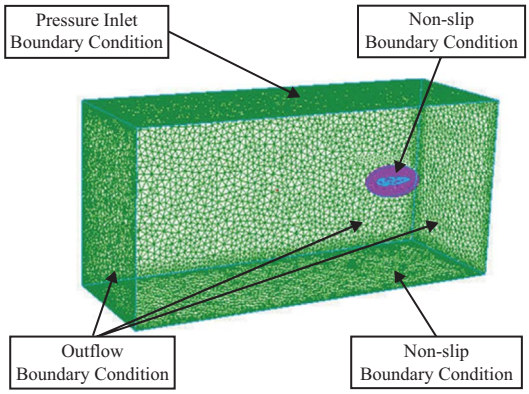

Fig. 10. Specification of boundary condition for AUV flow simulation.

flow field simulation of AUV, all the test cases in this study did not take account of the free surface effect on the vehicle. In reality, previous studies have shown that when a vehicle moves underwater at a depth three times its height (a condition satisfied by all the test cases in this study), the increase in total resistance on the vehicle created by wave-making resistance could be negligible [10]. Therefore, for the free surface, which denotes the intersection plane between water and air, the constant pressure inlet BC was chosen to simplify the time-consuming computation on this boundary. Additionally, the circumference of the computational domain were established as outflow boundary conditions. Fig. 10 shows the setting of the boundaries in the computational domain of the present study.

IV. RESULTS AND DISCUSSION

To evaluate the feasibility of using this simulation method to predict the effect of the control fin surface on the trajectory of the underwater vehicle, the flow field around the vehicle moving at a set depth was numerically simulated first to confirm the relationship between its motion resistance and sailing speed.

Fig. 11 shows a comparison of the surface pressure fields for an AUV under a specific dynamic sailing speed and different motion moments (1 sec and 10 sec). In this simulation, the test cases included three speeds (1 kt, 3 kt, and 5 kt), and the time step size Δt for the simulation was set at 0.01 sec for a total of 1,000 simulated time step vehicle movements over the simulated 10 sec. The calculation results shown in Fig. 11 indicate that a high pressure area gathers at the bow of the AUV during horizontal motion and changes to conform to the geometric shape of the AUV bow. The pressure distribution was inspected carefully. It appears that the pressure declines at the bow section and then increases again from the middle section to the stern. By calculating the difference between the pressure exerted on the AUV bow and stern, the form drag of the AUV moving in water could be determined. Furthermore, as indicated by the

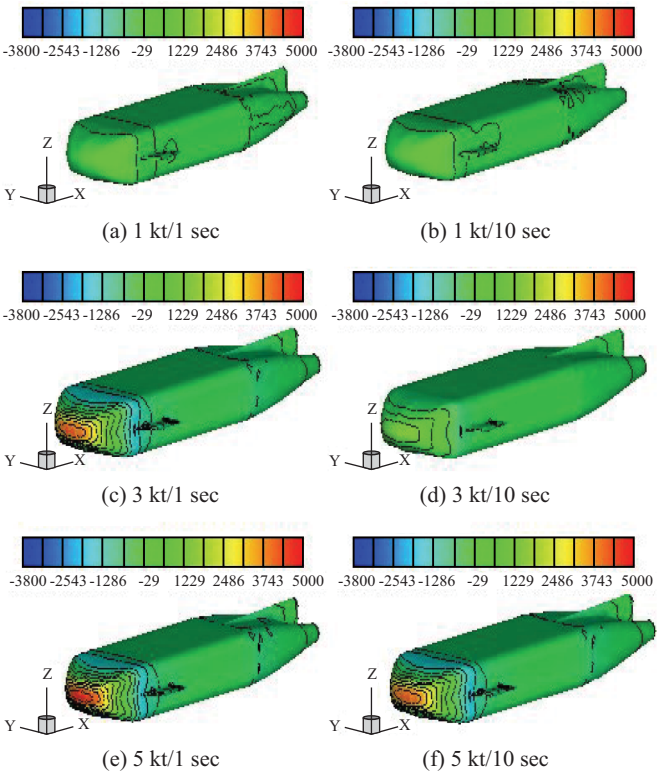

Fig. 11. Pressure contours around AUV at different moving speed.

comparison between pressures at different speeds shown in Figs. 11(a)-(f), the pressure at the bow increases as the speed increases. Therefore, the form drag on the AUV is higher at high speeds.

The dynamic resistance of an AUV at different speeds is shown in Fig. 12 and Table 2. Both demonstrate that regardless of the speed, an AUV bears the greatest resistance (including skin friction and form drag) at the moment as it moves from complete rest. These forms of resistance gradually decrease as the time of motion increases, until gradually being a constant value. Further examining the impact of different speeds on the ratio of change in the initial resistance dF_0 shows that dF_0 is greater at low speeds. The dF_0 value for an AUV at 1 kt, 3 kt, and 5 kt was 13.34%, 8.45%, and 6.80%, respectively. The definition of this resistance change ratio dF_0 can be expressed in Eq. (5):

$$dF_0 = \frac{|F_1 - F_0|}{F_0} \tag{5}$$

Here, F_0 represents the resistance against AUV at a certain time point T and F_1 represents the measured resistance at moment T + Δt. These simulated results also indicated that compared to high speed motion, when the AUV begins low speed motion from rest, it could experience larger resistance than once it achieves a steady speed. Additionally, as the changes shown in Fig. 12 and Table 2, although the fluid

Table 2. Records of dynamic resistance for AUV horizontal motion at different simulation time step (unit: N).

Time \ Speed	1 knot	3 knot	5 knot
1.0 sec	160.63	588.79	1188.85
2.0 sec	139.20	538.99	1107.93
3.0 sec	127.78	507.57	1067.94
4.0 sec	120.35	488.24	1038.45
5.0 sec	114.86	473.13	1013.15
6.0 sec	110.19	461.03	993.66
7.0 sec	106.65	452.14	979.32
8.0 sec	103.55	443.27	965.72
9.0 sec	101.13	437.08	955.89
10.0 sec	99.05	427.99	948.30

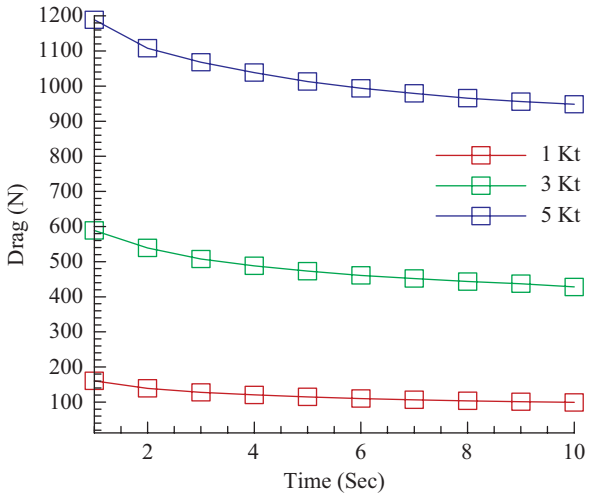

Fig. 12. Comparison of dynamic resistance for AUV horizontal motion at different speed.

resistance is greatest on the AUV immediately after it launches from rest, fluid resistance decreases as the sailing time increases. Using the simulated examples in this study, compared to the dF_0 between 1 and 2 sec, the dF_0 between 9 and 10 sec is significantly smaller, with 2.06% at 1 kt, 2.08% at 3 kt, and 0.79% at 5 kt. These simulated results explain that as the simulation time increases, and the AUV sails at the given speed, the fluid resistance would gradually become a set value.

After calculating the resistance for an AUV at the given speeds, this study further examined the effect of the changes of the control fin angle on the trajectory of AUV motion. To achieve the goal of dynamic motion simulation of AUV, the dynamic mesh technique was applied in this research topic. While employing this mesh technique, the flow field

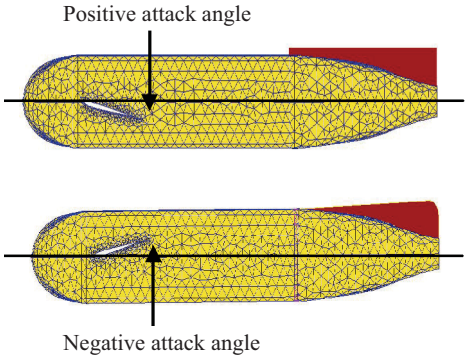

Fig. 13. Definition of attack angle of AUV's control fin.

meshes surrounding the AUV must conform the vehicle motion to regenerate the meshes. It should be noted, however, that the mesh regeneration or reconstruction significantly increases the simulation time. Because of computer resource limitations, this study only examined five simulation cases with AUV thrusts equal to 2000 newtons and control fin angles α of 0°, +5°, +10°, -5°, and -10°. Positive and negative attack angles for control fin surface rotations are shown in Fig. 13.

These simulation cases demonstrate that when the sailing speed of AUV equals 5 kt, the sailing resistance is approximately 1000 newtons. To analyze the effect of the control fin angle on AUV motion ability at higher speeds, the AUV was given 2000 newtons of thrust, enabling it to rapidly reach 5 kt from rest. After the AUV was given the specified thrust, it accelerated forward, gradually increasing speed. However, because of the proportional relationship between the fluid resistance and the vehicle's velocity squared, the speed and resistance simultaneously increased. The increasing resistance would gradually lessen the vehicle's acceleration as the time of motion increased. Once the acceleration approaches zero, it means that the fluid resistance approximates the value of thrust and the vehicle itself will move with a constant speed.

The centroid of the AUV significantly affects its motion ability. To set the motion coordinates and the centroid, this study defined the x axial direction as the bow-stern direction on the AUV, whereas the y axial direction as the port-starboard direction and the z axial direction as the water depth. The definition of the axial directions of the coordinate system is showed in Fig. 11. In this coordinate system (x, y, z), the positions of the AUV bow, stern, and centroid are (-2.1949, 0, -20.0059), (2.3051, 0, -20.0059), and (-0.1091183, 0, -20.00558) respectively. If the bow is used as the reference point, the AUV centroid locates at the position of 0.46351 vehicle-lengths from the bow in the study case.

Tables 3-7 compare the effect of the different attack angles of the control fin on the changes of fluid dynamic forces and rotating moments acting on AUV. In contrast to the simulation example shown in Fig. 11, the results shown in Tables 3-7 use a smaller time step Δt = 0.001 sec in order to

Table 3. Records of fluid dynamic forces and moments acting on AUV at different simulation time; attack angle α = 0°.

Time (sec)	Force (N)			Moment (N · m)	
	F*x*	F*y*	F*z*	M*x*	M*y*
0.2	234.232	-9.083	0.280	0.057	-0.660
0.4	250.955	0.439	-0.592	-0.063	8.409
0.6	291.628	-2.945	-8.554	-0.231	3.203
0.8	320.096	85.821	8.635	-1.136	2.504
1.0	380.675	56.404	4.046	-0.716	10.164

Table 4. Records of fluid dynamic forces and moments acting on AUV at different simulation time; attack angle α = +5°.

Time (sec)	Force (N)			Moment (N · m)	
	F*x*	F*y*	F*z*	M*x*	M*y*
0.01	220.403	-0.078	9.964	-0.059	9.319
0.02	200.999	-0.254	11.329	0.018	1.966
0.03	221.978	2.384	11.480	0.128	6.835
0.04	222.485	0.997	10.611	-0.290	9.445
0.05	233.291	9.559	11.975	-0.647	9.750
0.06	247.005	13.440	288.971	-1.824	406.533
0.07	227.897	18.005	702.645	-2.218	892.343
0.08	281.234	18.511	10084.83	-11.132	7841.344

Table 5. Records of fluid dynamic forces and moments acting on AUV at different simulation time; attack angle α = +10°.

Time (sec)	Force (N)			Moment (N · m)	
	F*x*	F*y*	F*z*	M*x*	M*y*
0.01	236.665	-0.042	18.985	0.019	32.768
0.02	223.088	-0.129	17.044	0.037	31.854
0.03	228.629	-0.703	-225.455	-0.999	-342.68
0.04	233.541	-9.632	-1190.969	-0.194	-1437.20

precisely compute the motion quantities of translation and rotation. The vehicle had different angles of attack on the control surface in various simulation examples. In general, the larger the angle of attack, the more likely that a negative-volume mesh would result from excessive torsion of the flow field mesh. Then, as the situation of radical motion happens, the simulation would stop due to the generation of high high-skewed meshes surrounding the AUV. Thus, the available simulation time listed in Tables 3-7 is different during the simulation. In the data presented in Tables 3-7, F*x*, F*y*, and F*z* represent the fluid dynamic forces exerting on the AUV in the axial directions *x*, *y*, and *z*, and M*x* and M*y* represent the corresponding rotating moment on the *x* and *y* axes, using the centroid as the reference point.

Table 6. Records of fluid dynamic forces and moments acting on AUV at different simulation time; attack angle α = -5°.

Time (sec)	Force (N)			Moment (N·m)	
	F*x*	F*y*	F*z*	M*x*	M*y*
0.01	220.297	-0.152	-10.032	0.009	-9.508
0.02	200.547	-0.149	-10.963	0.052	-1.229
0.03	223.330	-0.073	-12.631	0.066	-2.899
0.04	219.599	9.228	-10.803	0.782	-9.057
0.05	234.704	7.136	-11.272	0.361	-11.206
0.06	261.002	13.294	-270.141	1.283	-390.391
0.07	236.489	13.675	-862.057	4.057	-1086.32
0.08	294.042	-0.021	-14230.28	10.231	-9263.57

Table 7. Records of fluid dynamic forces and moments acting on AUV at different simulation time; attack angle α = -10°.

Time (sec)	Force (N)			Moment (N · m)	
	F*x*	F*y*	F*z*	M*x*	M*y*
0.01	231.960	-0.042	-21.624	-0.031	-14.024
0.02	222.861	-0.063	-17.569	-0.051	-31.372
0.03	229.364	0.852	245.928	0.755	353.74
0.04	213.267	-0.625	1085.477	3.113	1306.17

Compared to other attack angle simulations, the results in Tables 3 show that when the AUV attack angle equals 0° and the simulation time is 1 sec, the dynamic forces F*z* exerted on the *z* direction is still small. Therefore, the AUV could maintain horizontal motion along the *x* axis without any significant rotation. However, by further comparing the differences among these simulation cases, F*z* is positive as the attack angle is positive and it is negative as the attack angle is negative during the initial motion. It is obvious that larger F*z* values would likely result in the rotational moment M*y*. Then, under such circumstances, the motion attitude would not parallel with the thrust direction. Thus the hydrodynamic pressure exerting on the upper and lower surfaces of the vehicle would vary significantly to provide the enough moment to overturn the vehicle. This variance produces even higher values of F*z* and M*y*, causing the vehicle to rotate dramatically. This situation is identical to throwing a tissue horizontally. If the tissue does not maintain the horizontal motion, it often tips over quickly.

Figs. 14(a) and 14(b) show the simulation results of the attack angle α = +10° at simulation time 0.055 sec, and angle α = -10° at simulation time 0.056 sec respectively. Obviously, the motion posture of the AUV is dangerous and it is hard for any vehicle controller to accept the outcome. The causes for

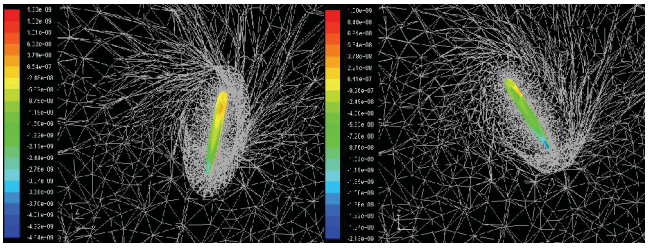

(a) (b)

Fig. 14. Influence of attack angle α on AUV's moving trace; (a) α = -10°/ t = 0.056 sec; (b) α = +10°/t = 0.055 sec.

this motion posture are the high sailing speed and excessive attack angle. Because the rotational angle of the control fin expanded steeply, the external mesh covering the AUV was overly skewed and could not conform the vehicle to regenerate meshes immediately so as to create negative volume meshes within the flow field. To avoid the problem mentioned above, the smaller time steps and finer meshes around the moving mesh block which envelopes the AUV should be used in the computational framework. However, such operating procedure would significantly increase the simulation time in the study.

V. CONCLUSIONS

The control fin surface has a significant effect on the motion function of an underwater vehicle. By changing the rotational angle of the fins, the underwater vehicle can adjust its lift, further changing its depth of motion in the water. As clearly demonstrated in this study, at high speeds, large rotational angles on the control fin surface can easily produce exaggerated rotational motion in an instant. Because of computer resource limitations, large amounts of simulation results for AUV motion prediction are not be presented in the present study. Despite being unable to further examine the relationship between speed change corresponding to the attack angle of the fin and its effect on the vessel's motion posture, this study identified the basic characteristics of the impact of the control fin on AUV's motion posture and verified the availability of the CFD analysis for underwater vehicle research.

REFERENCES

1. Atlas Maridan, Retrieved March 15, 2011 from http://www.maridan.atlas-elektronik.com/index. php?id=2267.
2. Chen, B. X., "New combat capability unmanned underwater vehicle," *Navy Professional Journal*, Vol. 43, No. 6, pp. 106-116 (2009).
3. Chen, H. C., Lin, W. M., and Hwang, W. Y., "Turbulent flow induced by multiple-ship operation in confined water," *Proceeding of the 15th ASCE Engineering Mechanics Conference*, pp. 1-8 (2002).
4. Chen, H. C., Patel, V. C., and Ju, S., "Solutions of Reynolds-averaged Navier-Stokes equations for three-dimensional incompressible flows," *Journal Computational Physics*, Vol. 88, No. 2, pp. 305-336 (1990).
5. Chen, J. L., Chen, C. H., Lou, D. W., and Wen, C. C., "The 3D numerical simulation for a miniature underwater vehicle with low Reynolds numbers," *Proceeding of the 10th Underwater Technology Conference and Result Presentation of National Science Council*, pp. 1-8 (2010).
6. Fluent Inc., *FLUENT 6.3 User's Guide*, Lebanon, NH (2006).
7. Gessner, T., *Dynamic Mesh Adaption for Supersonic Combustion Waves Modeled with Detailed Reaction Mechanisms*, Ph.D. Dissertation, University of Freiburg, Freiburg, Germany (2001).
8. Kao, C. H., "The development status and future trend of unmanned underwater vehicle," *Journal of Ocean and Underwater Technology*, Vol. 13, No. 3, pp. 9-17 (2003).
9. Lin, C. C., *Numerical Study of Tank Wall Effect on Torpedo Flow*, Master Thesis, Master Program of Naval Architecture and Ocean Engineering, Chung Cheng Institute of Technology, National Defense University, Taoyuan, Taiwan (2006).
10. Liu, T. L. and Huang, Z. W., "Numerical flow simulation and resistance analysis for submerged body moving under free surface effect," *Proceeding of the 11th National Computational Fluid Dynamics Conference* (2004).
11. Liu, T. L. and Lei, C. Y., "Numerical modeling of a three-dimensional moving torpedo flow and its underwater resistance analysis," *Proceeding of the 12th National Computational Fluid Dynamics Conference*, pp. 1-7 (2005).
12. Pan, T. H. and Huang, S. C., "The design and analysis of small underwater vehicle," *Journal of Engineering Technology and Education*, Vol. 7, No. 5, pp. 731-744 (2010).